FINAL PROGRESS REPORT

(1/15/99 – 1/15/2000)

BASIC STUDIES OF NONLINEAR OPTICAL MATERIALS FOR EYE AND SENSOR PROTECTION

PRINCIPAL INVESTIGATOR: PROF. PETER M. RENTZEPIS

Department of Chemistry
University of California
Irvine, CA 92697-2025
(949) 824-5934
pmrentze@uci.edu

REPORT DOCUMENTATION PAGE

Form Approved
OMB NO. 0704-0188

Public reporting burden for this collection of information is estimated to average 1 hour per response, including the time for reviewing instructions, searching existing data sources, gathering and maintaining the data needed, and completing and reviewing the collection of information. Send comment regarding this burden estimates or any other aspect of this collection of information, including suggestions for reducing this burden, to Washington Headquarters Services, Directorate for information Operations and Reports, 1215 Jefferson Davis Highway, Suite 1204, Arlington, VA 22202-4302, and to the Office of Management and Budget, Paperwork Reduction Project (0704-0188), Washington, DC 20503.

1. AGENCY USE ONLY (Leave blank)	2. REPORT DATE 1/20/2000	3. REPORT TYPE AND DATES COVERED Final Progress Report (5/15/96 - 1/15/2000)

4. TITLE AND SUBTITLE
Basic Studies of Nonlinear Optical Materials
for Eye and Sensor Protection

5. FUNDING NUMBERS

6. AUTHOR(S)
P. M. Rentzepis, P. Chen, I. V. Tomov, A. S. Dvornikov and D. A. Oulianov

DAAH04-96-1-0162

7. PERFORMING ORGANIZATION NAMES(S) AND ADDRESS(ES)

University of California
Irvine, CA 92697

8. PERFORMING ORGANIZATION REPORT NUMBER

9. SPONSORING / MONITORING AGENCY NAME(S) AND ADDRESS(ES)

U.S. Army Research Office
P.O. Box 12211
Research Triangle Park, NC 27709-2211

10. SPONSORING / MONITORING AGENCY REPORT NUMBER

ARO 35087.1-CH

11. SUPPLEMENTARY NOTES
The views, opinions and/or findings contained in this report are those of the author(s) and should not be construed as an official Department of the Army position, policy or decision, unless so designated by other documentation.

12a. DISTRIBUTION / AVAILABILITY STATEMENT

Approved for public release; distribution unlimited.

12 b. DISTRIBUTION CODE

13. ABSTRACT (Maximum 200 words)

We have studied the basic spectroscopy, kinetics and nonlinear optical properties of a set of power limiting materials, which include six metallobenzoporphyrins and ten donor-acceptor azulenic molecules. These compounds are known to have highly polarizable π-electrons, and therefore are expected to have nonlinear coefficients suitable for utilization in optical limiting devices. In order to diagnose the optical limiting properties of the materials, we developed new two-dimensional Z-scan technique. This technique allows us to measure separately real and imaginary parts of the third order nonlinear susceptibility $\chi^{(3)}$ of the materials, using arbitrarily beam shaped laser pulse and arbitrary sample thickness. In addition, the beam profile evolution anywhere inside the optical limiting material can be extracted accurately using 2D Z-scan technique. We have tested this technique using Gaussian and non-Gaussian special beam distributions, thin and thick samples, and applied it to the molecules studied. Some of the molecules showed high nonlinear absorption and nonlinear refraction at the wavelength of the experiment 527 nm. We also build a new picosecond transient spectroscopy experimental system, which generates ~ 1 ps pulse and allows us to measure absorption differences as small as $\Delta A = 0.005$. We were able, also, to measure accurately the spectra, kinetics and cross sections of the transients, which appeared after light absorption by the molecules studied. Almost all of the molecules exhibit strong reversed saturable absorption in a wide segment of the visible spectrum, with fast subpicosecond response time and fast decay rate. We list all of the parameters that are important for power limiting application of the molecules and propose photochemical mechanism. The results of our study suggest that some of the molecules are quite suitable media for power limiters.

14. SUBJECT TERMS		15. NUMBER IF PAGES
		16. PRICE CODE

17. SECURITY CLASSIFICATION OR REPORT UNCLASSIFIED	18. SECURITY CLASSIFICATION OF THIS PAGE UNCLASSIFIED	19. SECURITY CLASSIFICATION OF ABSTRACT UNCLASSIFIED	20. LIMITATION OF ABSTRACT UL

NSN 7540-01-280-5500

Enclosure 1

Standard Form 298 (Rev. 2-89)

Page   **Table of Contents:**

I. Abstract:

We have studied the basic spectroscopy, kinetics and nonlinear optical properties of a set of power limiting materials, which include six metallobenzoporphyrins and ten donor-acceptor azulenic molecules. These compounds are known to have highly polarizable π-electrons, and therefore are expected to have nonlinear coefficients suitable for utilization in optical limiting devices. In order to diagnose the optical limiting properties of the materials, we developed new two-dimensional Z-scan technique. This technique allows us to measure separately real and imaginary parts of the third order nonlinear susceptibility $\chi^{(3)}$ of the materials, using arbitrarily beam shaped laser pulse and arbitrary sample thickness. In addition, the beam profile evolution anywhere inside the optical limiting material can be extracted accurately using 2D Z-scan technique. We have tested this technique using Gaussian and non-Gaussian special beam distributions, thin and thick samples, and applied it to the molecules studied. Some of the molecules showed high nonlinear absorption and nonlinear refraction at the wavelength of the experiment 527 nm. We also build a new picosecond transient spectroscopy experimental system, which generates ~ 1 ps pulse and allows us to measure absorption differences as small as $\Delta A = 0.005$. We were able, also, to measure accurately the spectra, kinetics and cross sections of the transients, which appeared after light absorption by the molecules studied. Almost all of the molecules exhibit strong reversed saturable absorption in a wide segment of the visible spectrum, with fast subpicosecond response time and fast decay rate. We list all of the parameters that are important for power limiting application of the molecules and propose photochemical mechanism. The results of our study suggest that some of the molecules are quite suitable media for power limiters.

1

II. Summary of Accomplishment:

During the past three years (1996-1999) five paper on power limiting materials have been published and another is prepared for publication. Several presentations were made at National and International meetings. The principal investigator, Professor P. M. Rentzepis was awarded the Distinguished Faculty Award and Mr. Peilin Chen, received the Outstanding Chemistry Graduate Student Award. One graduate student, Peilin Chen, received his Ph.D. degree and accepted a position at the University of California, Berkeley and another, Dmitri Oulianov, has started research leading to his Ph.D. degree under the auspices of the ARO grand. Carlos Capanera received his BS degree in Chemistry while working part-time in the laboratory. In addition, Drs. I.V. Tomov and A.S. Dvornikov were involved part-time in this basic research project. In addition a patent application has been submitted on our two-dimensional Z-scan technique.

During this period we have developed a new two-dimensional Z-scan technique, an optical limiting materials diagnostic method. Using this method one can extract accurately real and imaginary parts of the third order nonlinear susceptibility $\chi^{(3)}$ of the material studied. In addition, the evolution of a beam profile anywhere inside the nonlinear device can be determined. Unlike conventional Z-scan, which requires strictly Gaussian beam distribution and thin samples, our 2D Z-scan technique can use arbitrary shaped beams and any "practical" sample thickness. This is very important advantage for the application of our method to the investigation of power limiting materials, because the laser beams, which if ever used for eye and sensor destruction, most probably will be of non-Gaussian distribution. We have successfully applied the 2D Z-scan to measurements of nonlinear parameters of several nonlinear molecules, such as metallobenzoporphyrins and azulenic donor-acceptor molecules. Several of these molecules have considerable nonlinear optical properties and could be suitable for optical limiting applications.

We have also studied the photochemistry of several metallobenzoporphyrins by means of picosecond transient absorption spectroscopy using experimental system, which generates 35 ps pulse. The transient spectra, kinetics and transient absorption cross sections of these molecules were measured and the light photochemistry mechanism was determined. Some of the molecules showed nonlinear absorption in the visible spectrum, and may be suitable for use as optical limiting media.

We have also build a new picosecond time resolved transient absorption spectrometer, which has ~ 1 ps time resolution and allows us to measure absorption differences as small as $\Delta A = 0.005$. Using this experimental system we have measured accurately transient spectra and kinetics of ten azulenic molecules in condensed media. Based on the experimental data we have proposed a mechanism for the photochemistry of these molecules. All of the molecules have intense and wide transient absorption band in 450-650 nm region, which makes them suitable for power limiting application.

In this, final progress report, we summarize our work for a period of 1996-1999 and list all of the data relevant to optical limiting applications of the molecules studied. This data could be used for the selection of materials suitable for power limiting applications and for guidance to future synthesis of materials with even better nonlinear properties.

2

III. Introduction:

In order to develop an effective optical limiter, there are two important issues to be considered: the search of the ultimate nonlinear optical (NLO) materials, and the capability of the optimization of optical limiting device. Currently, the most effective NLO materials are those compounds which exhibit large excited state absorption. However, there are no suitable means for the optimization of the configuration of optical limiting device. To study these two important aspects of the optical limiter, we have utilized picosecond and nanosecond transient spectroscopy to study the kinetics and mechanism of the NLO media, which allows us to understand the origin of the optical nonlinearity. In addition, we measured the absorption cross sections of the ground and excited states of all the NLO materials we studied. We have also developed a novel two dimensional Z-scan technique which allows to analyze the beam propagation inside the optical limiting devices. These measurements serve as powerful tools for the optimization of the instrumental parameters of optical limiter including the thickness and the geometry of the NLO materials, and the figure of merit[1] which is defined as the ratio of the linear transmittance to the minimum transmittance for the attainable excited state population.

Organic materials with large π conjugated systems are often used as NLO media because of their large nonlinear absorption cross sections and fast optical response. With proper synthetic techniques, these organic NLO materials can be tailored to meet one or more of the required parameters, for example, the wavelength and decay rate. One of the major applications for this type of NLO materials is the active component of the optical limiter whose function is to limit the light transmitted through the device to lower levels than the damage threshold of optical sensors or human eyes. There are several mechanisms which are responsible for the operation of an optical limiter. Among them, the NLO materials which exhibit reversed saturable absorption (RSA) have been shown to be very promising. Recently, several NLO materials with large RSA[2-6] have been synthesized and are considered to be used in the optical limiting devices. It has been demonstrated that with these types of materials, nonlinear attenuation up to 10^4 is no longer inaccessible. When these types of materials are excited to an upper electronic state, the absorption coefficients between the excited states are much larger than those in the ground states, which effectively increases the effective absorption coefficient as the incident laser energy increases. Therefore, the transmitted light is highly attenuated. The response time of this effect can be as fast as few femtoseconds and the decay time depends on the lifetime of the excited molecules. To employ RSA materials in an optical limiter, the NLO materials should exhibits following properties[7-8] : The absorption cross section of the excited molecules must be much higher than that of the ground state molecules, and the lifetime of the excited state should be longer than the incident laser pulse duration in order to accumulate the population in the excited state. However, it should become transparent shortly after the incident laser pulse. In order to be effective against a wide range of wavelengths, the optical limiting materials should exhibit a broadband transient absorption which covers the entire visible region. Before we try to use NLO materials in the optical limiter, we must check that they satisfy these criteria. Therefore, we need to

study the kinetics of the NLO materials and measure their excited state absorption coefficients at the wavelengths where the device must absorb.

Porhyrins, and Azulene-containing donor-acceptor compounds are two classes of compounds which possess large delocalized π electrons, and it has been shown that these two classes of compounds may exhibit the desired nonlinear optical properties. In this report, we will present the nonlinear, two photon absorption spectra of all excited states as a function of delay time and input laser power. The formation and decay rates of the excited states were measured by means of picosecond and nanosecond time resolved spectroscopy and the absorption cross-sections of all relevant transitions were derived from the experimental data. This information allows us to calculate the population and magnitude of the absorption cross section for each transition, at a given power and any interval of time. The excited state spectra and kinetics provide the necessary data for describing in detail the photochemical mechanism which in turn helps to guide us toward the synthesis of the optimum material for eye and sensor protection.

We also present the means for measuring the optical nonlinear parameters of these two classes of NLO materials. These measurements were performed by our new technique, which is based on a two-dimensional Z-scan and split step beam propagation method (BPM), which allows us to extract the beam propagation profile within an optical limiting device. With the capability of measuring the beam profile inside the nonlinear media, this method may also be used for the optimization of figure of merit in the optical limiters. Although we concentrated our studies on NLO materials which exhibit excited state absorption, our technique can be extended to the study of any NLO material. To evaluate the capability of the nonlinear attenuation for these two classes of materials, we also have measured their nonlinear transmission with picosecond pulses.

Ever since its introduction, the Z-scan technique has been widely used to study nonlinear optical phenomena because of its experimental simplicity and easy to use[9-10]. Using the original Z-scan configuration, both the real and imaginary parts of the third order nonlinear susceptibility, $\chi^{(3)}$ of the NLO materials, can be easily determined by means of the "open" and "close" aperture Z-scan plot. The original Z-scan formulation was derived under the assumption of Gaussian beam shape and thin sample approximation. To extend the application of the Z-scan technique, several modifications have been made. Top-hat beam[11-12] and eclipsing Z-scan[13] were used to enhance the sensitivity of the Z-scan, and optically thick materials[14-16] were utilized to increase the signal. A recent study[17], however, has shown that even with a slightly deviation from a perfect Gaussian beam distribution, the Z-scan curve will give erroneous optical nonlinear parameters. Most of the modified Z-scan techniques deduce the nonlinear optical parameters from a spatially and temporally averaged signal. In practice, the incident beam distribution which impinges upon the optical limiters is not Gaussian, but most likely resembles, closely, top-hat beams. In order to improve the optical limiting devices further, the development of techniques, which allows one to analyze the evolution of the beam profile during its propagation inside the optical limiting device, are highly desirable.

The information obtained in a typical Z-scan experiment is only one dimensional. Recently, Marcano[18-19] et al utilized the CCD as the detector for Z-scan experiments. CCD is a two-dimensional array detector, therefore, it has several advantages when used in Z-scan experiments: a) the distribution of both signal and reference beams can be obtained simultaneously. b) the image recorded is digitized and stored in a computer after data acquisition, therefore, the image is ready to be further processed and analyzed. c) the dynamic range of the CCD detector is very high (up to 2^{16}), and its pixel size may be as small as a few μm. The physical size of the CCD detector allows to record the whole far field distribution of the laser beam during the Z-scan experiment. Since the far field distribution of signal and reference beams can be recorded simultaneously, the input beam distribution is not subjected to the limitation of a certain beam shape. However, to obtain the optical nonlinear parameter, $\chi^{(3)}$, a general formulation for the Z-scan experiment must be used.

The original Z-scan techniques apply only to a perfect Gaussian beam and thin sample which, in practice, are not suitable for optical limiter devices. To diagnose and design an optimal optical limiter, it is very important to know the evolution of the beam distribution inside the device. In our experiment, we have employed a CCD camera to record the far field pattern in Z-scan experiments which use both CS_2 and porphyrins as NLO materials. In order to calculate the far field pattern we applied the beam propagation methods[20-22] to solve the nonlinear Maxwell equation. This method is valid for any arbitrary beam shape and thickness of the sample. Both near field and far field patterns can be calculated with small amount of computation time. This allows us to calculate the two dimensional beam profile for each Z-scan step, and compare the simulation results directly with the experimental data which are recorded by a two dimensional CCD detector. This technique offers a simple but accurate means for the evaluation of the beam distribution inside the optical limiting devices. In addition, this technique encompasses all the Z-scan modifications reported so far. We also present the nonlinear data obtained for several of the azulenic compounds and Zn tetraphenyltetrabenzoporphyrin.

We have also studied the photochemistry of several metallobenzoporphyrins by means of picosecond transient absorption spectroscopy using experimental system, which generates 35 ps pulse. The transient spectra, kinetics and transient absorption cross sections of these molecules were measured and the light photochemistry mechanism was determined. Some of the molecules showed nonlinear absorption in the visible spectrum, and may be suitable for use as optical limiting media.

We also present the results of time-resolved ultrafast spectroscopy for ten azulenic donor-acceptor molecules performed using our new experimental system with ~ 1 ps time resolution. With this time resolution we were able to measure the spectra, cross sections and kinetics of the transients accurately, which allowed us to propose a mechanism for the photochemistry of these molecules. All of the azulenes studied were found to exhibit similar kinetics. We have observed the development of a strong and wide RSA band within the excitation pulse, which then decays with a time constant of $3 - 59$ ps. The RSA band has its maximum at $450 - 650$ nm, a width of $40 - 100$ nm (FWHM) and a cross section at the absorption maximum of $2.85 - 13.3 \times 10^{-17}$ cm^2 , depending on the

5

molecule. Because of the fast response time ($\tau < 1$ ps), fast decay rate, high cross section and broadband spectrum of the RSA band, the azulenic molecules could be very useful for power limiting applications. For all of these molecules we also observed bleaching of the charge-transfer (CT) band and the development of a new absorption band in 750 – 850 nm region.

IV. Two-dimensional Z-scan:

a) Theory:

In this section we will, briefly, describe the two-dimensional Z-scan method, and present the theoretical model, which is described in more detail in reference [13]. Fig. 1 shows a schematic representation of the experimental system of the two-dimensional Z-scan. In order to extract the information from the two-dimensional far field pattern recorded by the CCD camera, the propagation of the beam through the sample has been simulated using the split step BPM[14-15]. The basic idea of the method is based on the solution of the scalar nonlinear Helmholtz equation numerically by writing it in the operator form. The input field distribution $E(x,y)$ at the entrance plane of the sample (plane 2, Fig.1) can be calculated from the experimentally measured intensity distribution $I(x_1,y_1)$ at the lens plane (plane 1, Fig.1) by the Frenel approximation of the Kirchhoff diffraction integral:

$$E(x,y) = h_0 \iint g(x_1,y_1) \exp(ik\frac{x_1^2+y_1^2}{2f})p(x_1,y_1)\exp\left[-ik\frac{(x-x_1)^2+(y-y_1)^2}{2d}\right]dx_1dy_1 \ , \tag{1}$$

where $g(x_1,y_1) = \sqrt{I(x_1,y_1)}$, $h_0 = \frac{i}{\lambda d}\exp(-ikd)$, f is the focal length, d is the distance between the entrance and lens planes, and $p(x_1,y_1)$ is the aperture function at the lens plane. The input intensity distribution $E(x,y)$ is used as an initial condition in BPM. The optical path of the beam inside the sample is divided into several small propagation steps Δz. The solution of the scalar Helmholtz equation for a single frequency three-dimensional wave for each propagation step Δz can be written as

$$E(x,y,z+\Delta z) = \hat{P}\,\hat{A}\,\hat{L}\,\hat{A}\,\hat{P}(x,y,z) \ , \tag{2}$$

where $\hat{P} = \exp\left(-ik_0n_0\frac{\Delta z}{2}\right)\cdot\exp\left\{-i\frac{\Delta z}{2}\left[\frac{\nabla_t^2}{(\nabla_t^2+k_0^2n_0^2)^{1/2}+k_0n_0}\right]\right\}$ is the propagation operator, $\hat{A} = \exp\left[-\alpha_{NL}(I)\frac{\Delta z}{4}\right]$ is the absorption operator; and $\hat{L} = \exp\left(-ik_0\int_z^{z+\Delta z}\delta n\Delta z\right)$ is the nonlinear refraction operator.

To evaluate the operator $\hat{P}$, we first take the Fourier transformation of the field to the spatial Fourier domain. The electric field can be expanded as the Fourier sum

$$E(x,y,z,t) = \sum_r \sum_s E_{rs}(z,t)\exp(-ik_{xr}x)\exp(-ik_{ys}y) \tag{3}$$

and the transverse derivative ∇_t^2 can be expressed for each component as $\nabla_t^2 = -(k_{xr}{}^2 + k_{ys}{}^2)$ where k_{xr} and k_{ys} are spatial frequencies in the two dimensional Fourier series which can be calculated efficiently by FFT. After the evaluation of $\hat{P}$, the electric field is transformed back to real space in order to evaluate $\hat{A}$ and $\hat{L}$, and then evaluate $\hat{P}$ again. To propagate Δz, we need to evaluate a series of $\hat{P}\hat{A}\hat{L}\hat{A}\hat{P}$ operators. Following this procedure the propagation inside the nonlinear medium can be calculated. The propagation from the exit plane of the sample (plane 3, Fig.1) to the detector plane (plane 4, Fig.1) can be calculated using the Frenel approximation of the Kirchhoff diffraction integral, as it was done for the case of propagation from the lens plane to the sample's entrance plane.

To calculate the nonlinear absorption coefficient α_{NL}, we have to set up the rate equation for a pulse traveling in the Z-direction. Since we used picosecond pulses in the experiment, the contribution from the triplet state can be neglected[16]. We also assume that the relaxation rate at the excited state manifolds are very fast compared with the pulse duration. Therefore, the rate equation can be written as

$$\frac{dS_0}{dt} = -\sigma_{01}S_0\Phi + K_{10}S_1 \tag{4}$$

$$\frac{dS_1}{dt} = -\sigma_{01}S_0\Phi - K_{10}S_1 \tag{5}$$

$$\frac{d\Phi}{dz} = -(\sigma_{01}S_0 + \sigma_{12}S_1)\Phi \tag{6}$$

where $\Phi = I/h\nu$ is the photon flux, and S_0, S_1 are the concentration of the ground and excited state. σ_{01}, σ_{12} are the absorption cross-section of the ground and excited state molecules. K_{10} is the rate constant from the excited singlet to ground state. The nonlinear coefficient α_{NL} is determined as:

$$\alpha_{NL} = \sigma_{01} \cdot S_0 + \sigma_{12} \cdot S_1 \tag{7}$$

In above formulation, the nonlinear effects are separated into two parts, absorptive and non-absorptive. The change due to the absorption is described by the nonlinear absorption coefficient α_{NL}, which can be calculated by the coupled rate equations. The change due to Kerr effect, nonlinear refraction and other effects are included in δn term. These nonlinear optical parameters can be derived by integrating the intensity of two-dimensional pattern with open or closed aperture.
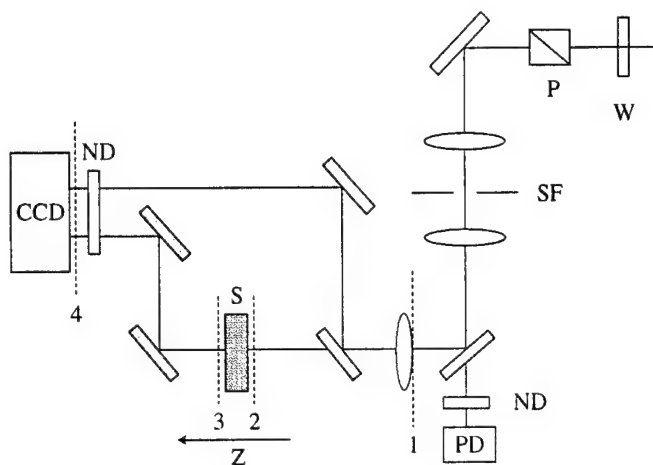
Fig. 1. Schematic diagram of the two-dimensional Z-scan experimental system: W - half wave plate; P - polarizer; ND - neutral density filter. PD - photodiode. 1 - lens plane; 2 - detector plane.

b) Experimental:

Fig.1 shows a schematic representation of the two-dimensional Z-scan experiment. The laser system uses a cw mode locked Nd:YLF laser, and a regenerative amplifier. The repetition rate of the regenerative amplifier can be adjusted between 40 to 1000 Hz by properly selecting the frequency divider in the Pockel cell. We have also used a mechanical shutter to perform single pulse experiments, which allow us to eliminate accumulative effects such as heating of the sample. In the experiments described in this report we used the second harmonic, 527 nm, 35 ps full width half maximum (FWHM) pulses, and the beam diameter was measured to be 1.7 mm (FWHM). The intensity of the second harmonic was adjusted, as needed, by a half wave plate and polarizer and various neutral density filters. When a Gaussian distribution pulse was used, for the Z-scan experiments, a spatial filter was employed to improve the beam shape quality. A beam splitter located after the focusing lens was used to reflect a part of the beam, which then used as a reference beam. The Gaussian beam was focused by a 220 mm focal length lens to a radius of 25 μm, which corresponds to confocal beam parameter $Z_0 = 3.7$ mm. The NLO materials were placed in either a 1 mm, or a 10 mm thick, quartz cell. The signal beam passed through the sample cell, while the reference beam propagated through the air and was appropriately attenuated to match the signal beam intensity before striking the detector. Both signal and reference beams were simultaneously recorded by a 16 bit 256 $\times$ 1024 pixels CCD detector (pixel size 26 μm, Princeton Instrument LN/CCD 1024EUV) situated 250 mm away from the focal point. In some measurements, reported here, a 2 $\times$ 2 binning was used, in this case the effective pixel size was 52 μm. Additionally the intensity of the input laser beam was also monitored by a calibrated Si photodiode. Fig. 2 shows a two-dimensional far field pattern of the reference beam.

When a top-hat pulse was used, the spatial filter in Fig. 1 was replaced by an expansion telescope, which consisted of a negative 35 mm focal length lens and a positive 250 mm focal length lens. A 3.75 mm diameter aperture was placed at the axes of the beam to form the top-hat beam used in the measurement. Fig. 3 shows the beam profile measured

8

250 mm away from the aperture. The variation of the intensity across the beam cross section was less than 20%, which is the result of diffraction. This beam was then focused by a 220 mm focusing lens for the Z-scan measurements. The focusing lens was situated 200 mm after the forming aperture.
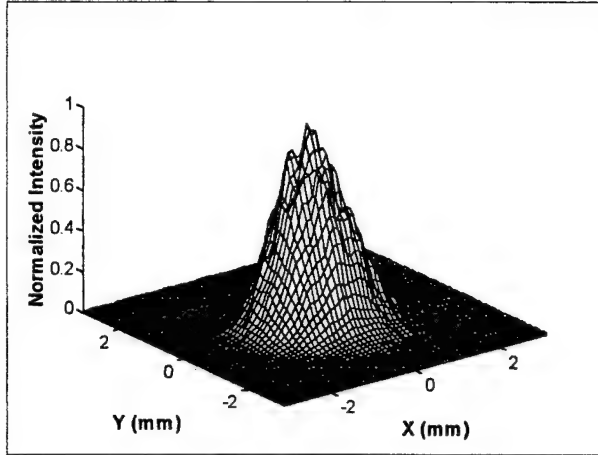

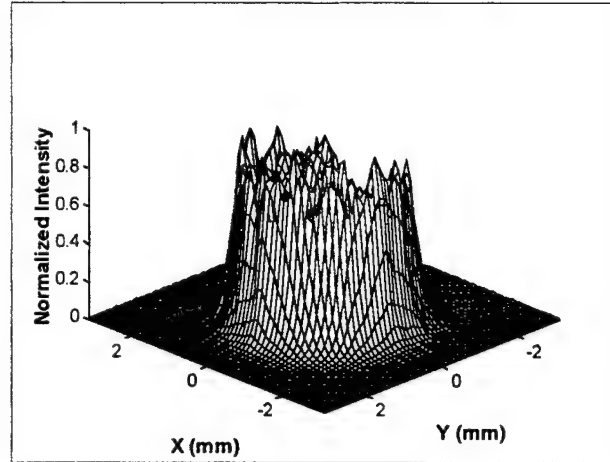Fig. 2. Far field beam profile of the reference beam, recorded by a CCD camera.

Fig. 3. Top-hat beam profile measured 250 mm away from the forming aperture.

A more stringent test of this method would be a strongly deformed laser beam. To form such a spatial beam distribution a Gaussian beam was sliced into two nonsymmetrical parts by placing a 0.8 mm diameter wire vertically close to the center of a Gaussian beam. Fig.4 shows the smoothed beam profile of the split Gaussian beam measured 50 mm away from the wire. The beam was focused by a 250 mm focal length lens which was located 15 mm after the wire. The diameter of the Gaussian beam before the wire was 1.4 mm (FWHM) and the confocal beam parameter without the wire was 7.4 mm.
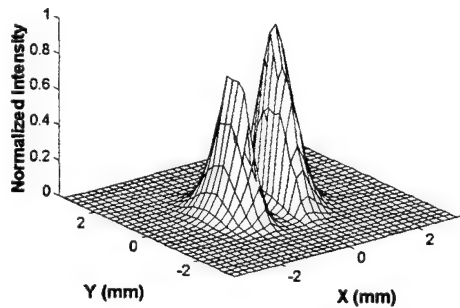

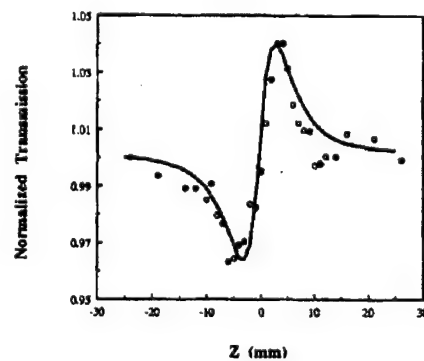Fig. 4. Split Gaussian beam profile measured 50 mm away from the wire

Fig. 5. Closed aperture Z-scan plot using a 1mm thick CS_2 cell, S=0.4. Points are the integrated signal from the CCD image. Solid line represents the integrated signal from the calculated far field beam profile by BPM.

9

c) Results and Discussion:

We first applied our two-dimensional Z-scan technique to study the well-known and experimentally studied nonlinear liquid, carbon disulfide in order to ascertain the accuracy of this method. The laser beam shape was very close to Gaussian with peak intensity of 1 GW/cm^2 at the focus. When the sample was illuminated by high repetition rates laser pulses (40-300 Hz), a cumulative thermal effect was observed. To avoid this effect the results presented here were obtained using single laser pulse for record in each frame. For each Z-position, eight frames of the far field pattern were recorded by the CCD detector. Beam walking can be minimized by fitting both reference and signal images with an elliptical Gaussian distribution and using the center from the fitting result instead of a fixed position. The intensity of each beam was determined by integration over the image, with a radius of 60 pixels, which covers about 99% of the overall energy of the laser beam. In the open aperture experiments, the fluctuation of the intensity ratio between reference and signal beams was less than 1% for all Z-positions. The data points shown in Fig. 5 represent the normalized intensity ratio between 40% of the center signal beam and the entire reference beam for a 1 mm thick sample . This corresponds to aperture size of S=0.4 in a typical Z-scan experiment. Using the original Z-scan formulation, we obtained $\gamma = (3.1 \pm 0.3) \times 10^{-14}$ cm^2/W, which agrees with the widely accepted value for CS$_2$ within experimental error. This showed that our method is valid and can be used to measure accurately nonlinear parameters of materials. To calculate the beam distribution for each Z-position, we used the BPM with all the experimental parameters and a 128 x 128 grid. The solid line in Fig. 5 is the corresponding simulation curve calculated by the split step BPM, while the points represent the experimental data. The fit between the calculated curve and experimental data is seen to be rather good.

To study optically thick materials, a 10 mm thick CS$_2$ sample was used. The thickness of the sample was almost three times larger than the Rayleigh length. To determine the beam profile changes induced by changes in the nonlinear index of refraction, we compared the beam profiles recorded by the CCD when the sample was in the focal area (where nonlinear effects are present) and when it was away from the focus (where nonlinear effects are absent). We subtract the image recorded when the sample is away from the focus from the image recorded when sample is in the focal area. The obtained difference is a measure for the changes in the beam profile due to nonlinear effects in the sample. Fig. 6 shows both the observed and calculated differences in the far field profiles for a 10 mm thick sample of CS$_2$. The difference is normalized to the reference beam intensity. Fig.6a displays the difference in the pre-focal area, when the entrance window of the cell was 5 mm before the focus, the intensity decrease in the center region indicates the defocusing effect. Fig.6b shows the focusing effect in the post-focal area, when the entrance window of the cell was 5 mm after the focus. The agreement of the calculated beam profile difference with the observed change proves that this technique is also quite accurate for the optically thick samples.

In addition we further applied our two-dimensional Z-scan technique to zinc tetraphenyl-tetrabenzoporphyrin (ZnTPTBP) which has been shown[7, 24] to exhibit high excited state absorption. ZnTPTBP was dissolved in tetrahydrofuran (THF) to 70% linear transmission
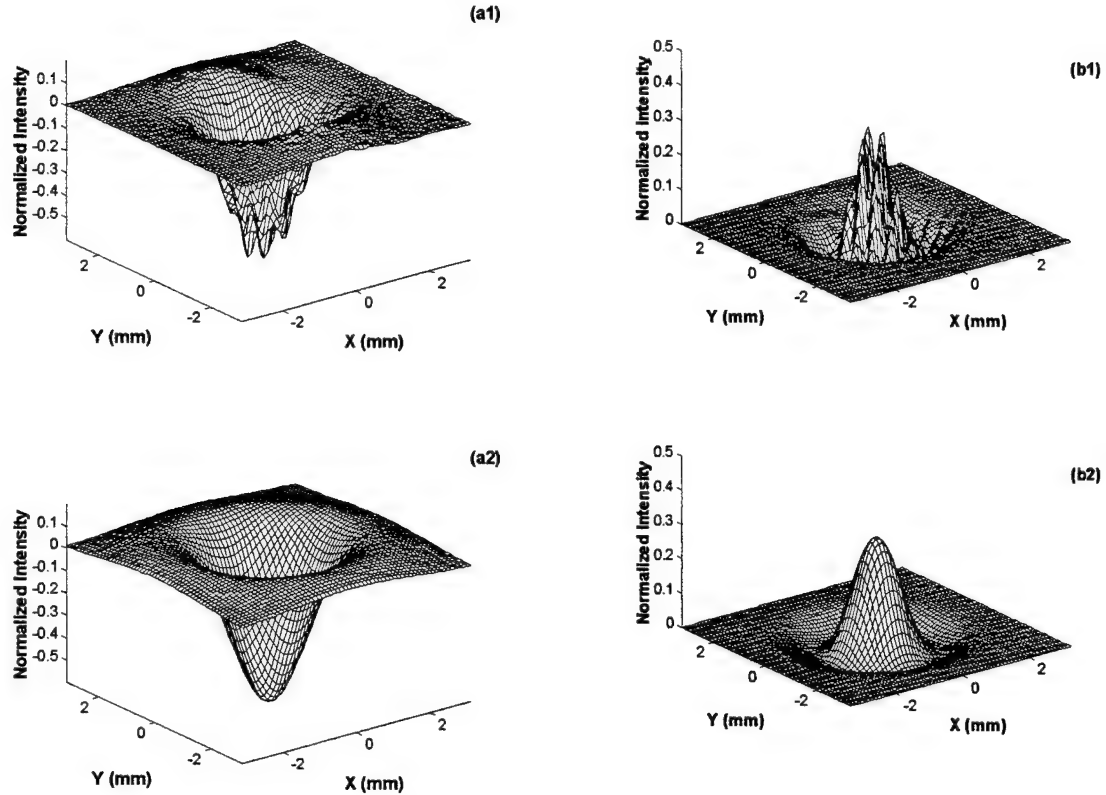
Fig. 6. Far field beam profile difference for a 10 mm CS_2 cell : (a1) measured difference at $Z = -5$ mm; (a2) calculated difference at $Z = -5$ mm; (b1) measured difference at $Z = 5$ mm; (b2) calculated difference at $Z = 5$ mm. Z is the position of the cell entrance window. Negative Z is before the focus which is situated at $Z=0$.

in a 1 mm thick cell. In the experiment the sample was scanned through the focus and images of the far field profile were recorded for each position. The recorded signal and reference images were integrated around their image centers within a 60 pixels radius. The intensity of the signal beam was then normalized using the reference beam and an open aperture Z-scan plot was obtained. This experimental result was compared with the calculated one. We simulated the same experimental conditions in the theoretical model by setting the grid size to be the same as the effective pixel size and used the published data[7] for ZnTPTBP, $\sigma_{01}=1.7 \times 10^{-17}$ cm^2, $\sigma_{12}=7.2 \times 10^{-17}$ cm^2. The calculated far field patterns were then processed by the same method as the experimental data. Fig. 7 shows the open aperture Z-scan plot for ZnTPTBP where the solid line is the calculated curve without any adjusting parameters and the points correspond to the experimental data. This figure shows that the simulation results agree very well with our experimental data. Using the same set of parameters as in the above simulation we can determine the beam propagation profile within the sample. Fig. 8 shows the evolution of the beam radius within the ZnTPTBP sample near the focal area. A strong nonlinear attenuation can be clearly seen at 1 mm distance after the focus. Note that if the nonlinear effects were absent the beam profile in the focal area will experience very small changes since the confocal parameter in this experiment was 3.7 mm. Using the same experimental set up,

11

when the sample was only pure solvent, we observed no changes in the beam profile. This indicates that the nonlinear contribution to the index was due mainly to the absorption of the ZnTPTBP molecules.
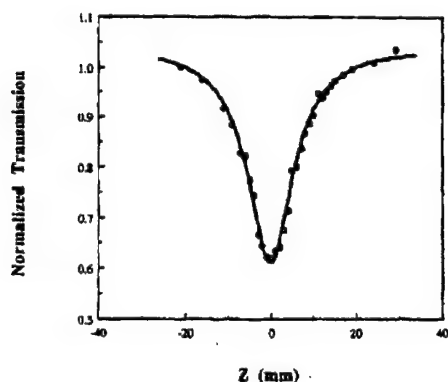

Fig. 7. Open aperture Z-scan plot using a 1 mm thick ZnTPTBP/THF solution. Data points represent the integrated intensity over the recorded far field pattern. Solid line is calculated by BPM.
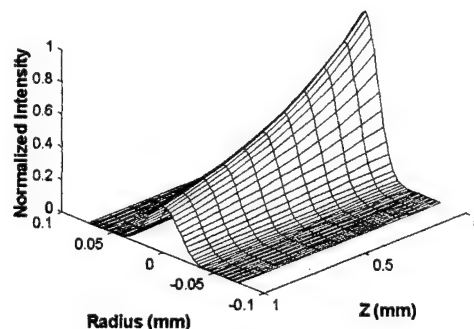
Fig. 8. Beam profile evolution inside a 1 mm thick ZnTPTBP/THF solution. The entrance plane to the NLO medium is located at Z = 0 mm

Recently, beams with top-hat shape had been successfully used in Z-scan experiments[11-12]. The advantage of using this type of beam shapes is that it overcomes the strict Gaussian beam limitation that was previously a stringent necessity for Z-scan experiments. Generally, the light from laser sources with non-Gaussian beam profiles can be expanded to form the top-hat beam, and then used in Z-scan experiments. It was also shown[11] that the use of top-hat beams increases the sensitivity of the experiment by a factor of 2.5. To extract the nonlinear optical properties of the sample from the Z-scan experiment with top-hat beams, however, the thin sample approximation was required. Our two-dimensional Z-scan method allows one to use beams with arbitrary shape and in addition, this method is not restricted to the thin sample approximation. In fact thick samples may be easily and accurately used. To verify these statements we used a beam with top-hat spatial shape and propagating through a 10 mm thick sample. Fig. 9 shows the observed and calculated far field pattern of a top-hat pulse propagating through a 10 mm thick CS_2 sample. A strong focusing effect was observed at the center of the beam profile. The entrance plane of the nonlinear materials was located at Z = 0 mm. The data show that there is a good agreement between calculated and observed beam profiles. The fine structure modulation observed in the experimental profile is due to the interference effects from the edge of the beam forming aperture (see Fig.3).

We also performed the same experiment using a split Gaussian beam distribution, as a more crucial example of the application of the two-dimensional Z-scan method to non-Gaussian beam distribution. In comparison with a top-hat beam shape, a split Gaussian beam distribution has no circular symmetry and it is difficult to calculate analytically the propagation of this beam through the nonlinear liquid. Fig. 10 depicts both the experimentally measured and calculated beam distribution in the far field for a split

12

Gaussian pulse after propagation through a 10 mm thick CS_2 cell. The entrance plane of the nonlinear material was located at $Z = 0$ mm. Integrating over the central circular parts of two peaks of the split Gaussian distribution in the far field we have calculated the closed aperture Z-scan curve. The radii of the integration circles were equal to each other and they covered 40% of overall energy. The points in Fig. 11 represent the experimental data and the solid line corresponds to the Z-scan curve calculated using the simulation method.
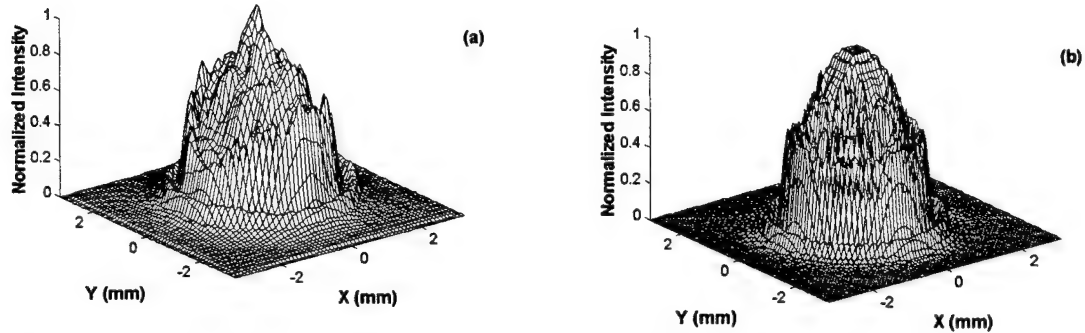

Fig. 9. (a) Observed far field pattern of a top-hat pulse propagating through a 10 mm thick CS_2 sample. (b) Calculated far field beam profile for the top-hat pulse. The entrance plane to the NLO medium is located at $Z = 0$ mm.
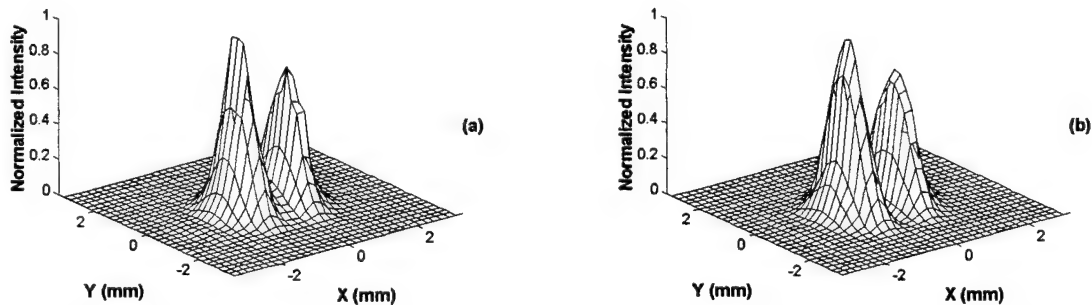

Fig. 10. Observed far field pattern of a split Gaussian pulse propagating through a 10 mm thick CS_2 sample. (b) Calculated far field beam profile for the split Gaussian beam. The entrance plane to the NLO medium is located at $Z = 0$ mm.

The γ values measured for all three beam profiles with thick and thin CS_2 samples, were the same within the accuracy of the experiment. The accuracy of the measurements was determined, mainly, by the uncertainty in obtaining the peak intensity within the focal area, since small diffraction related disturbances were always present.

In the original Z-scan experiment, an aperture is placed at the far field, and by measuring the transmittance as a function of the sample position (Z), the nonlinear index of refraction can be calculated. However, there are several difficulties in the use of this type of setup for the diagnoses of optical limiters. First, a Gaussian distribution beam is required which may not be the case for most optical limiter applications. Second, beam
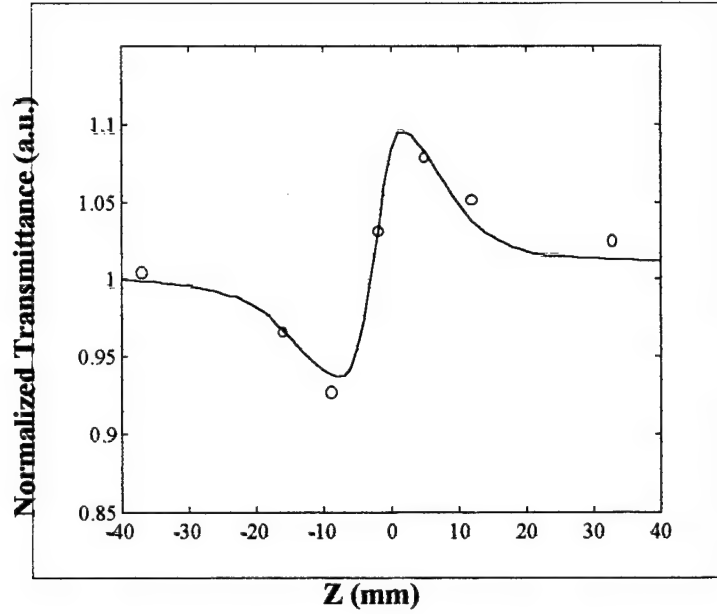
13

Fig. 11. Closed aperture Z-scan plot of a 10mm thick CS_2 for a split Gaussian beam distribution. Points represent the integrated signal from the CCD image, and the solid line represents the integrated signal obtained from the calculated far field beam profile by BPM.

walking, and fluctuation in the beam shape during the experiment add to the difficulty in obtaining accurate data. Third, even a small amount of absorption will modify the refractive index of the medium, which will then complicate further the interpretation of the Z-scan data. In our two dimensional Z-scan method, all these difficulties have been eliminated: A CCD detector was used to record the beam profile of both the interrogating and reference beams at the same time. This simultaneous recording allows for the compensation of beam walking and beam profile fluctuation during the experiment. A mechanical shutter was utilized to perform single shot experiments which when compared with high repetition rate data make it possible for us to estimate the heating and other effects induced by the large number of pulses propagating through the sample at a short period of time. With the aid of the beam propagation method, the evolution of beam distribution for any beam shape can be calculated directly from the experimental data at any position inside the optical limiting device.

Studies have shown that in order to increase the dynamic range of the optical limiters, more complicated geometries for these devices are needed such as tandem[25] and graded density[26] limiters. Our method may be used, in these and other arrangements, to study both theoretically and experimentally the beam behavior inside the optical limiting devices and consequently determine the optimum concentration distribution for any given geometry. These parameters can be determined by simply replacing the initial constant concentration (S_0, S_1 in equation (4-6)) with a concentration distribution, which can be optimized numerically for any given parameter or condition. The behavior of the beam profile inside any optical limiting device may be determined experimentally with this technique by inverting the observed far field patterns.

14

The experiments presented here show that there is a very good agreement between the measured and calculated two-dimensional far field beam profiles of Gaussian, top-hat and split Gaussian pulses after propagation through various materials in both thin and thick cells. We believe these studies show that the experimental technique in conjunction with the split step BPM can be used to calculate propagation of any arbitrary beam shape inside the nonlinear material with any thickness with good accuracy. The experiments have also demonstrated that the Z-scan curves calculated from the simulation results fit the experimental data very well for both closed and open aperture Z-scan results. Thus the two-dimensional Z-scan method is quite suitable for the measurements of most nonlinear properties of materials with high accuracy. In addition this method if properly use may also be a powerful tool for the design of optical limiters.

After the success of this technique with carbon disulfide and benzoporphyrin we employed the two-dimensional Z-scan method to study six azulenic derivatives (molecules **1-5** in Fig.12). The experimental setup was the same as the one that we used for carbon disulfide and bensoporphyrin. .Normally, for each Z-position of the cell 24 to 32 frames were measured. For each frame, we calculated the energy of each beam by integrating the signal and reference images over the areas with 60 pixel radius, which cover 99% of the overall energy. Then, we averaged the energy ratio of the signal and reference beams over the frames that correspond to the same Z-positions of the cell. The plot of the normalized energy ratio (normalized transmittance) vs. the Z-position of the cell is referred to as the open aperture result, from which the index of nonlinear absorption can be determined. The index of nonlinear refraction was measured by integrating the image of the signal beam over a circular aperture that contains 40% of the overall energy and then we divide the result by the energy of the reference beam. After averaging over the frames corresponding to the same Z-positions of the cell and normalization we obtain the so-called closed aperture result (with aperture parameter $S=0.4$), from which one can calculate the index of nonlinear refraction. In order to calculate indexes of nonlinear refraction and nonlinear absorption, the closed and open aperture graphs were fitted to the theoretical curves that were calculated using Gaussian decomposition methods[9]. We first calibrated the system with a nonlinear liquid, carbon disulfide, whose nonlinear index of refraction is well known. Then we performed the same measurements with the materials under study. For these measurements all azulenic samples were dissolved at a concentration equivalent to 70% transmission at 527 nm in a 1mm thick cell. The indexes of nonlinear refraction and nonlinear absorption for carbon disulfide and azulenic compounds **1-5** were measured using the two-dimensional Z-scan technique. These data are listed in Table 1. It is evident that, at the wavelength of the experiment, $\lambda=527$ nm, the azulenic compounds show positive nonlinear refraction for compound **3, 5** and negative for compounds **1, 2** and **4**. The values of the nonlinear index were found to vary from $0.7 \cdot 10^{-14}$ cm^2/W for compound **5** to $-7.5 \cdot 10^{-14}$ cm^2/W for compound **2**, which is more than twice the magnitude of the nonlinear index of CS_2. For compounds **1-3** we did not observe nonlinear absorption, while compound **4** has the nonlinear absorption index of $7.1 \cdot 10^{-9}$ cm/W. Compound **5** showed negative nonlinear absorption, which can be explained by bleaching of the charge transfer band in the ground state spectrum of **5** (for more details see section VII of this report).

Tabel 1: Nonlinear coefficients measured by two-dimensional Z-scan technique

Molecule	γ (nonlinear refraction index) at 527 nm	β (nonlinear absorption index) at 527 nm
CS_2	$3.1 \cdot 10^{-14}$ cm^2/W	no absorption
1 [a]	$-5.2 \cdot 10^{-14}$ cm^2/W	no absorption
2 [b]	$-7.5 \cdot 10^{-14}$ cm^2/W	no absorption
3 [b]	$2.1 \cdot 10^{-14}$ cm^2/W	no absorption
4 [c]	$-2.6 \cdot 10^{-14}$ cm^2/W	$7.1 \cdot 10^{-9}$ cm/W
5 [b]	$0.7 \cdot 10^{-14}$ cm^2/W	$-2.9 \cdot 10^{-9}$ cm/W

[a] in dichloroethane
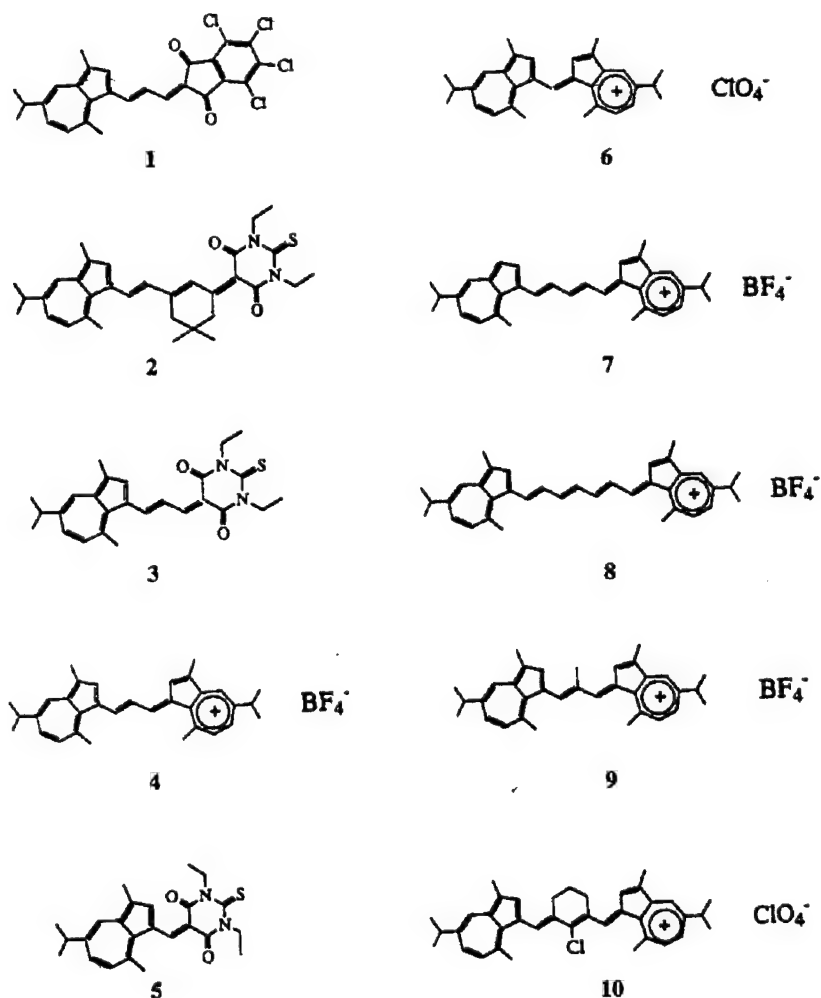[b] in dichloromethane
[c] in methanol

Fig. 12: Chemical structure of azulene-containing donor-acceptor molecules studied

16

V. Picosecond Transient Spectroscopy of Bensoporphyrins:

a) Experimental:

In the picosecond transient spectroscopy, a passive mode-locked Nd:YAG was used as the oscillator. A single pulse was selected by a Pockels cell which was split into two parts and amplified by two double pass amplifiers. The pulse duration for the fundamental line was about 35 picosecond. The output from the first amplifier was focused by a 15 cm focal lens into a 15 cm cell filled with a mixture of H_2O and D_2O, to generate picosecond continuum, followed by another lens to recollimate the continuum beam. An ND 1 filter and a Corning 4-69 filter were used to select continuum in the range of 400 nm to 800 nm. The continuum was then split by a 50% beam splitter to two parts, one part was used to probe the solution containing the sample and the other passed through the reference cell containing pure solvent. The signal and the reference beams were focused onto the slit of a spectrograph with 6 mm separation distance. A liquid nitrogen cooled 256 x 1024 pixels CCD detector (Princeton Instruments) was mounted on the output of a spectrograph. Two sections of the CCD with 20 x 1 binning (1 pixel binning along wavelength axis) were used to record the sample and reference signals. The spectrometer was calibrated with a Hg lamp. When the second harmonic radiation was used for excitation, a Raman notch filter was placed in front of the spectrograph to block the second harmonic scattered light.

The output from the second amplifier was converted to second harmonic in a KDP crystal with about 3 mJ energy. A KG3 filter was used to filter out the fundamental radiation. The excitation beam was then focused by a 1 m lens to a 2.5 mm diameter spot. For kinetic measurements, all the benzoporphyrin samples were dissolved in benzene at a concentration equivalent to an absorbance of 0.5 - 1 at 532 nm in a 1 cm optical path cell ($\sim 10^{-4}$ M). The excitation energy was monitored by means of a Molectron J-4 energy meter. The kinetic measurements were performed at the region where there was no saturation effect, namely at low excitation energy. For each data point, two consecutive measurements were made, one with and the other without excitation. Together with the reference spectrum, four spectra were used to calculate the transient absorbance. This procedure minimized the possible energy fluctuation in the continuum. Normally 80 shots, per spectrum, were averaged and used to calculate the absorbance, and the transient spectra were further smoothed by 5-point averaging.

b) Results and Discussion:

In this study, we studied six benzoporphyrins : zinc meso-traphenyltetrabenzoporphyrin (ZnTPTBP), copper meso-tetra(p-methoxy-phenyl)tetrabenzoporphyrin (CuTMPTBP), nickel meso-tetraphenyl- tetrabenzoporphyrin (NiTPTBP), nickel meso-tetra(p-methoxyphenyl)-tetrabenzoporphyrin (NiTMPTBP), platinum meso-tetraphenyltetra-benzoporphyrin (PtTPTBP) and platinum meso-tetra(p-methoxyphenyl)-tetrabenzoporphyrin (PtTMPTBP). We investigated the transient spectra and kinetics of these six different benzoporphyrin derivatives by means of picosecond transient spectroscopy. This technique has been well established for the study of transient species[27]. The advantages of this technique are : First, the time resolution is the same as

17

the laser pulse duration which can be as short as tens of femtosecond. Second, unlike fluorescence measurements, this technique can be applied to probe radiationless transitions and absorption spectra. Third, with a CCD detector, both spectra and kinetic information can be obtained simultaneously.

Porphyrin and phthalocyanine derivatives have been reported to exhibit reverse saturable absorption properties[3, 6, 28], however, the optical limiting power among these derivatives were quite different. Therefore, it is important to know the substitution effects on optical limiting through the kinetic and spectroscopic studies. The nonlinear optical properties of some meso-substituted benzoporphyrins have been reported lately, and the excited state absorption was found to be the dominant factor for their nonlinear properties. Our data showed that the energy relaxation process of the meso-substituted benzoporphyrins studied were quite different. For Zn and Pt benzoporphyrins, the transient absorption lasted as long as nanoseconds, but for Ni and Cu benzoporphyrins, the transient absorption disappeared within 100 ps. It is our goal to understand the relationship between the excited state kinetics and the optical nonlinear properties in benzoporphyrins.

In general, porphyrins with D_{4h} symmetry (planar configuration) exhibit two main transitions in the UV-Visible region, a weak visible Q-band and a strong near-UV, B (Soret), band[29]. Different substitutions change the position of these bands, but the separation between the Q-band and B-bands remains roughly the same. The tetrabenzoporphyrins showed red-shifted spectra compared with porphyrins because of more delocalized p electrons on the macrocycle. Table 1 shows the B-band and Q-band absorption maxima and the molar absorption coefficients for all the benzoporphyrins we investigated. The molar absorption coefficients of excited states were measured at 40 ps time delay intervals. The absorption origins were different for different benzoporphyrins, and detail assignments will be presented in the following section.

1) ZnTPTBP :
Previous transient measurements[30-31] of Zn porphyrin derivatives showed that the lifetime of the excited singlet states were about 2.5 ns. These transient spectra have characteristic $^1(\pi,\pi^*)$ and $^3(\pi,\pi^*)$ absorptions which exhibit very strong absorption between the ground state B-band and the Q-band bleachings. Rodriguez et al[31] pointed out that the transient spectra in this region were not distinguishable because of band overlapping. However, the $^1(\pi,\pi^*)$ level exhibits a unique Q(0,1) stimulated emission which should be at the same position as the spontaneous Q(0,1) emission, and the $^3(\pi,\pi^*)$ transition can be marked by the distinct near infrared absorption peak. Fig. 13 shows the transient spectra of ZnTPTBP at various time delays. A strong transient absorption at 500 nm was observed. The dip in the absorption band around 532 nm was due to the Raman notch filter used to eliminate the scattered second harmonic light. After a fast rise, the intensity of the transient absorption maximum remained at the same absorbance for about 5 nanoseconds, but shifted slightly to the red at longer time delay. This behavior is the same as the one observed in the zinc tetraphenylporphyrin (ZnTPP). The transient absorption maximum and absorption coefficients of the excited singlet states
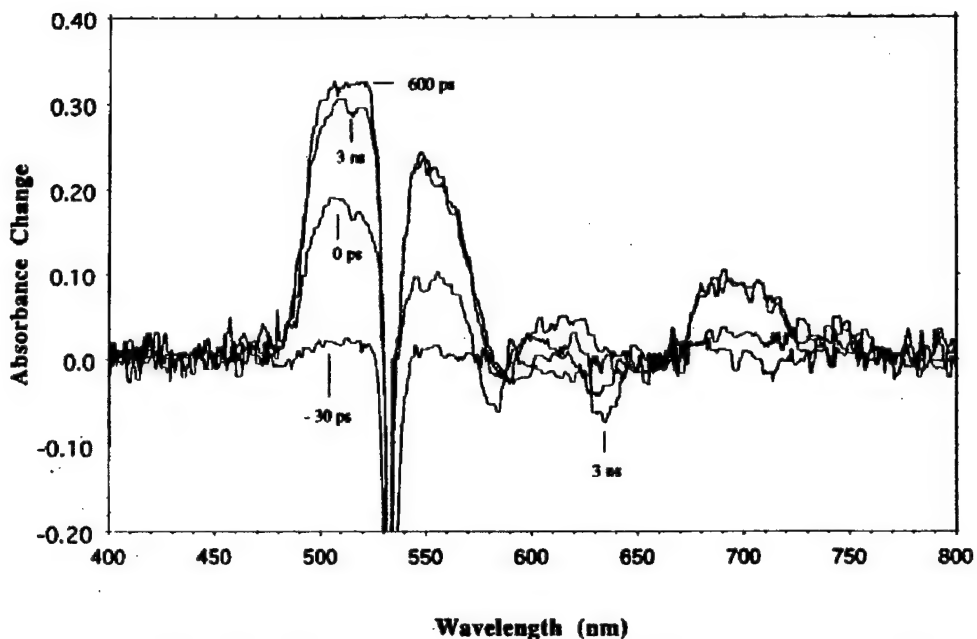
18

Fig. 13. The transient spectra of ZnTPTBP in benzene at various time delays.

and triplet states were very close to those found in ZnTPTBP. It was practically impossible to extract any useful information in the 500 nm region. In order to evaluate the relaxation time of the excited states we have looked for their characteristic behaviors, the Q(0,1) stimulated emission and the near infrared absorption. We did not observe any stimulated emission in our experiments, probably because of the low emission intensity of the Q(0,1) benzoporphyrins band and of the low continuum intensity at the wavelengths longer than 720 nm owing to the Raman notch filter. However, we did observe the transient absorption of the excited singlet state around 600 nm and determined the lifetime of the excited singlet state to be 650 picoseconds. We also observed a slowly rising component around 700 nm which is the characteristic absorption of the triplet state. From the data of ZnTPTBP in benzene, we know that the lowest excited singlet state exhibits a broad band absorption which extends to 600 nm, and a lifetime of less than 1 nanosecond. The lowest excited triplet state also has its absorption maximum in the 500 nm region, however, it has a characteristic absorption in the 700 nm region that reaches its maximum absorption intensity after 1 nanosecond.

2) CuTMPTBP :

Cu (II) has an unpaired d-electron which interacts with the porphyrin π electrons. As a result of this coupling the energy levels of this porphyrin are modified[32]. Under these condition the ground state becomes a singdoublet $^2S_0$, and the lowest excited singlet state becomes singdoublet $^2S_1$. Alternatively, the triplet states $^3(\pi,\pi^*)$ split into tripdoublet $^2T(\pi,\pi^*)$ and quartet $^4T(\pi,\pi^*)$. Because of the admixing between the excited singdoublets into the tripdoublets by exchange interactions, an additional transition was observed for CuTMPTBP around 920 nm. Kobayashi et al[33] reported that the relaxation process for Cu
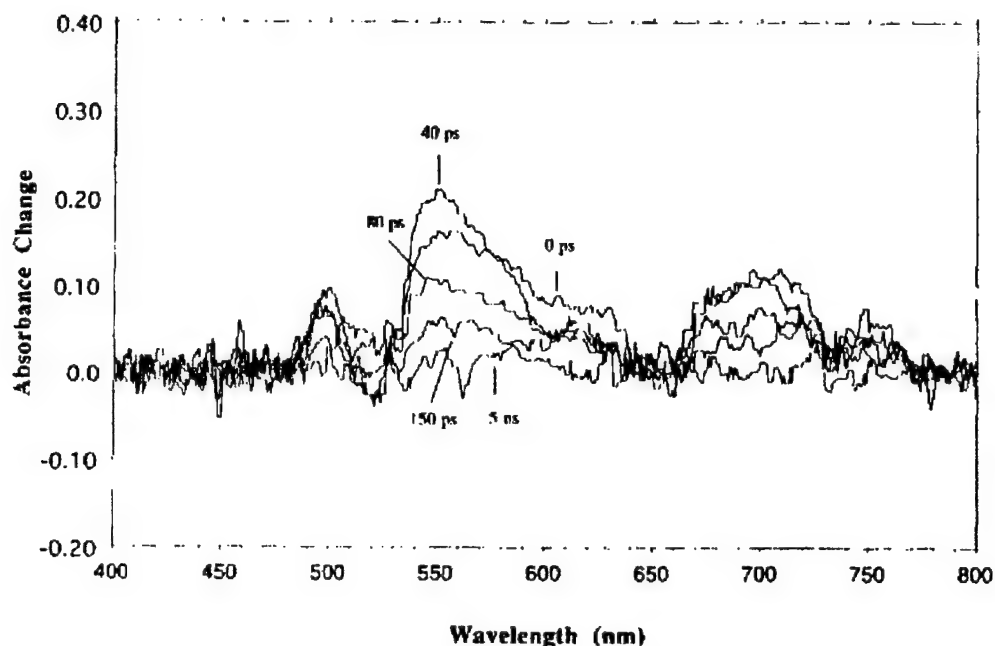
19

Fig. 14. Transient spectra of CuTMPTBP in benzene at various time delays.

protoporphyrin IX dimethyl ester (CuPPDME) was from the lowest excited singdoublet state $^2S_1$ to the lowest tripdoblet $^2T(\pi,\pi^*)$ within 8 ps and then to a thermal equilibrium state between $^2T(\pi,\pi^*)$ and $^4T(\pi,\pi^*)$ with a time constant of 450-460 ps. Using phosphorescence measurements at room temperature, the lifetime of the $^2T(\pi,\pi^*)$ component of the thermal equilibrium state was estimated to be longer than 1 ns[34]. However, kinetic measurements of copper tetraphenylporphyrin (CuTPP) and Cu(Etio) in toluene showed that the transient absorption and bleaching were dominated by two components, a major component which lasted for more than 10 ns and a smaller absorption component which relaxed in less than 500 ps[35]. The relaxation of the excited singdoublet state $^2S_1$, was believed to relax to tripdoublet $^2T(\pi,\pi^*)$ within the excitation pulse duration and the major component was assigned to the transient absorption of the ^2T and/or ^4T state. In our studies of CuTMPTBP, only one major relaxation rate was determined. There may be a weak component which lasts more than 1 ns. However, the amplitude of this weak component was too small for accurate kinetic evaluation. Fig. 14 shows the transient absorption spectra of CuTMPTBP, after excitation with a 532 nm pulse. The kinetics of this band are composed of an instrument limited rise time and a relative fast decay (~ 50 ps) , Fig. 15. The transient absorption spectrum of CuTMPTBP is very similar to that of ZnTPTBP, except that the absorption maximum is shifted to the red. At zero time delay the spectrum exhibited an absorption peak around 550 nm and a weak red tail extended to 650 nm. The red-tail was only observed at zero time delay and may be attributed the absorption of the $^2S_1$ state which relaxed to tripdoublet $^2T_1$ state within the pulse duration. Kim et al[35] indicated the absorption of $^2T_1$ and $^4T_1$ states were roughly the same, and 50 ps relaxation time of the 550 nm absorption band may be attributed to the relaxation of thermal equilibrium state of $^2T_1$ and $^4T_1$.

20

Compared with the relaxation time of other Cu porphyrin derivatives in noncoordinated solvents, 50 ps is too fast for the relaxation of the equilibrium state. A reasonable explanation is the formation of dimers or aggregates[36,37] which contain more charge-transfer character than monomer and lead to a fast inter-system crossing process. In this study we did not identify the existence of the dimers.
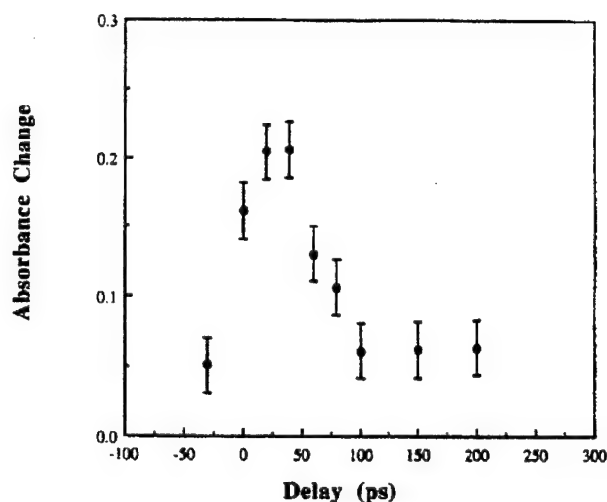

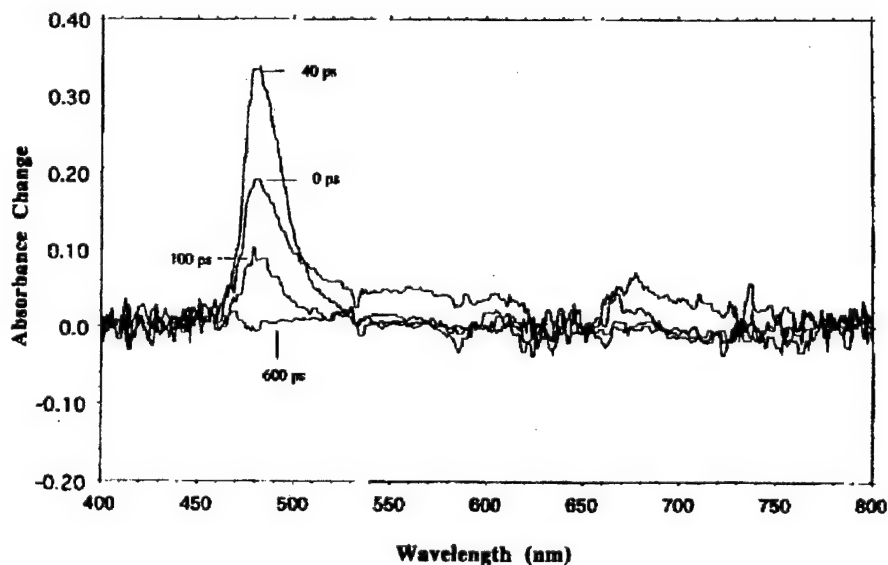Fig. 4. The kinetics of CuTMPTBP at 550 nm.

Fig. 5. Transient spectra of NiTPTBP in benzene from 0 ps to 600 ps.

3) NiTPTBP and NiTMPTBP :

The electronic configuration of Ni (II) is d^8, the lowest three d-orbitals, d_{xy}, d_{yz}, d_{xz} are always filled up with electrons when incorporated into porphyrins. Depending on the number of coordination, the last two electrons can either fill up the d_{z^2} or occupy both the d_{z^2} and the $d_{x^2-y^2}$ orbitals. Ake and Gouterman[38] showed that in four-coordination

21

Ni porphyrins, the electron configuration of the ground state is $(d_z2)^2$. Previous measurements showed that there were two relaxation processes for the transient of nickel protoporphyrin dimethyl ester (NiPPDME)[30], one with 10 ps and the other with 250 ps lifetime. Because there are many possible relaxation pathways through the low-lying metal state, different investigations have led to different conclusions[30,39-41]. Recent studies of Ni porphyrins concluded that for NiTPP in noncoordinated solvents[42], the energy was transferred from the initial excited $^1Q(\pi,\pi^*)$ state which is localized on the macrocycle to the low-lying metal $(d_z2, d_x2_{-y}2)$ state within 350 fs. And the macrocycle returned to its ground state configuration in the same period of time. However, the excess energy increased the internal vibrational energy which was responsible for the change in transient absorption for the first 20 ps. The lifetime of the low-lying metal state was about 250 ps. They also pointed out that the (d, d) excited states exhibited two characteristic spectral features : a sharply featured spectrum near 350-600 nm and the absence of absorption in the red. When the Ni tetrabenzoporphyrin derivatives were dissolved in benzene, the transient spectra showed a strong absorption at 480 nm. Fig. 5 shows the transient absorption spectra of NiTPTBP in benzene. The transient spectrum exhibited a relatively sharp absorption maximum compared with other tetrabenz-porphyrin derivatives except at zero time delay where the spectrum extended to the red. In NiTPP and NiPPDME these red tail absorptions were also observed and therefore, they may be associated with the unrelaxed vibrational components. In general, the transient absorption of Ni tetrabenzoporphyrin derivative possessed the characteristic (d, d) absorption, a sharp absorption maximum between Soret and Q band and an absorption at the red of the ground state bleaching (around 650 nm). Therefore, the relaxation process for both Ni porphyrins are through the low-lying metal state. The lifetime of this low-lying metal state is about 45 ps for NiTPTBP and 65 ps for NiTMPTBP.

Table 2: Absorption coefficient

Molecule	B-band		Q-band		Excited state	
	λ_{max}, nm	ε, mM^{-1}cm^{-1}	λ_{max}, nm	ε, mM^{-1}cm^{-1}	λ_{max}, nm	ε, mM^{-1}cm^{-1}
ZnTPTBP	462	224	652	47	510	19
CuTMPTBP	467	131	647	43	550	11
NiTPTBP	448	220	643	88	480	10
NiTMPTBP	453	200	643	71	480	9
PtTPTBP	429	76	613	47	470	11
PtTMPTBP	435	43	613	25	460	8

4) PtTPTBP and PtTMPTBP :

As the atomic number of the metal core of porphyrins increases we expect that the inter system-crossing rate will also increase. It is known that Pt porphyrins do not fluoresce but phosphoresce. All the measurements of Pt porphyrins[43,44] showed that the lifetimes of the excited singlet states were less than 10 ps and the transient absorption in the pico-nanosecond time scale are mainly due to $^3(\pi,\pi^*)$ absorption. In our study, both PtTPTBP

and PtTMPTBP transient spectra showed characteristic $^3(\pi,\pi^*)$ absorption, a broad absorption maximum between Soret and Q band and a weak absorption at the red of Q band absorption. The intensity of the transient absorption maximum remained the same up to 5 ns. Therefore, we conclude that the lifetimes of the excited singlet state for both PtTPTBP and PtTMPTBP are less than the pulse duration and the transient absorption we observed belongs to the triplet-triplet transition.

Table 3: The absorption cross sections at 532

Molecule	σ_{01}, x10^{-17} cm^2	σ_{12}, x10^{-17} cm^2
ZnTPTBP	1.7	7.2
CuTMPTBP	3.0	4.3
NiTPTBP	1.5	1.6
NiTMPTBP	2.0	2.3
PtTPTBP	1.7	3.4
PtTMPTBP	1.3	2.1

VI. Picosecond spectroscopy of azulenes:

a) Experimental:

A schematic representation of the experimental system used for transient absorption spectra and ultrafast kinetics measurements is shown on Fig. 17. For our measurements we employed a subpicosecond laser system, which consists of a mode-locked Ti:sapphire laser (Tsunami from Spectra-Physics) coupled to a regenerative amplifier (Spitfire, Spectra-Physics). The output of the regenerative amplifier consisted of 1.6 ps pulses at 1 kHz repetition rate and a wavelength centered at 840 nm. The fundamental beam was frequency doubled to give the 420 nm pulse used for excitation. This pump pulse was separated from the fundamental by a dichroic beamsplitter and focused behind the sample by a 1000 mm focal length lens. The pump pulse energy was, typically, 60-100 μJ, and the beam diameter, in the sample, was equal to 1 mm. In order to generate a picosecond supercontinuum pulse a part of the fundamental beam was focused into a cell containing deionized water. The spectrum of the supercontinuum was found to cover the 430-840 nm wavelength range. The continuum beam was recollimated after the cell and split into two beams to form the probe and reference beams. The probe beam was focused to a 0.1 mm diameter spot inside a 1 mm thick sample cell by a 250 mm focal length lens and was intersected by the pump beam. The reference beam passed through a 1 mm reference cell, which contained the same solution as the sample cell. The probe and reference beams were focused onto the slit of a monocromator. A 16 bit 256x1024 pixels CCD detector (pixel size 26 μm, Princeton Instrument LN/CCD 1024EUV) was mounted at the output end of the monochromator and was used to monitor the spectra of the probe and reference beams. We utilized 120 pixel vertical binning to form two horizontal strips, which cover the spectra of the probe and reference beams. To measure the kinetics the arrival of the probe pulse in the cell was delayed by a certain period of time with respect to the pump

pulse. For each delay time, two consecutive measurements were made, one with excitation and the other without excitation. Together with the reference, four spectra were used to calculate the transient absorption spectrum. This procedure minimized the possible energy fluctuations in the continuum. For the measurement of each spectrum, usually 10,000 pulses were averaged. With this experimental system absorbance changes as small as 5×10^{-3} were observed and resolved. For calibration of the system we used 1.9×10^{-2} M chloranil/acetonitrile solution, because its transient state absorption spectra, cross section and kinetics are well known[45-46]. For the kinetics measurements described here, the azulenic samples were dissolved in dichloromethane or acetonitrile to an absorbance of 0.1–0.3/mm at 420 nm.
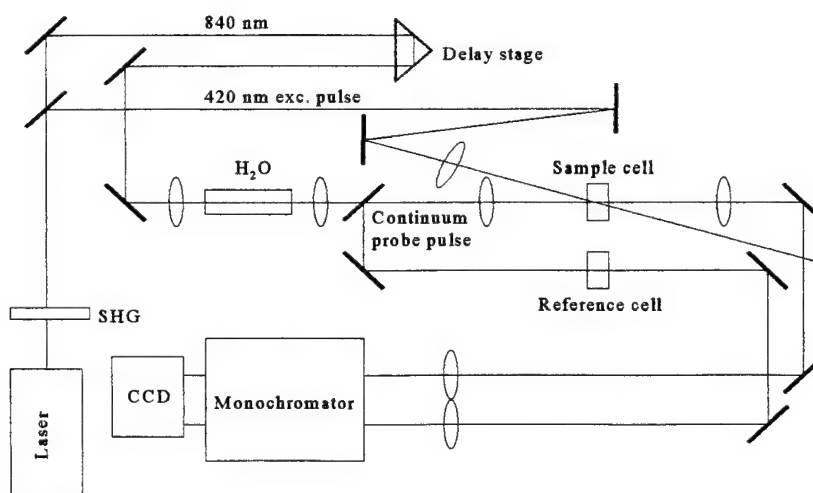

Fig.17: Schematic diagram of the experimental system for subpicosecond transient absorption spectra and kinetics measurements.

b) Results and Discussion:

The chemical structures of ten azulenic donor-acceptor molecules, which we studied and discussed in this report, are shown in Fig. 12. These molecules are known to have highly polarizable π electron groups, and therefore could have high nonlinear constants and optical properties required for optical limiters[47-51]. The ground state electronic spectra of all of the azulenic samples studied were found to have a very intense absorption band in the visible region, which is attributed to a charge-transfer transition. For most of these compounds the CT band maximum is located in the red region of the visible spectrum. It is known that the CT spectrum shifts towards the infrared with increase in conjugation. The location of the CT band as expected depends, strongly, on solvent polarity (see Table 1). In the experiments described here, the CT absorption band was excited with a 420 nm picosecond laser pulse and subsequently the spectra and kinetics of the excited transient states were recorded. All of the molecules exhibit the same kinetics. As an example,

Table 4: Ground state absorption for azulenic derivatives (λ_{0max} – maximum of charge-transfer absorption band; ε - extinction coefficient for the charge-transfer band)

Molecule	λ_{0max}(nm)					ε $(10^4,cm^{-1}M^{-1})^{b,*}$
	A	b	c	d	e	
1		649	n/s	632		7.38
2	602	642	651	625	627	5.97
3	573	634	636	594	629	8.28
4		772	761	764	757	24.27
5		546	544	527		4.74
6	n/s	690	682	684	678	10.60
7		876				24.10
8		987				27.50
9		774				17.40
10		916				22.20

a: in cyclohexane
b: in dichloromethane
c: in ethanol
d: in tetrohydrofuran
e: in acetinitrile

n/s: not soluble

*: data provided by Prof. A. E. Asato, University of Hawaii

Fig.18 shows the change in absorbance of molecule **6** at several time intervals before and after excitation. In these transient spectra we can identify bleaching of the CT band and the formation of two new absorption bands shifted to the blue (band **I**) and to the red (band **II**) relative to the CT band. The maximum absorbance of band **I** is at 500 nm, the bleaching maximum is located at 690 nm, which coincides with the maximum of the CT band, and the maximum of band **II** is at 750 nm. Band **II** partially overlaps with the strong CT band, therefore its "real" maximum could not be seen and may be it is shifted to the blue. The kinetics measured at the maximum of the absorption bands **I** and **II**, and at the maximum of the CT band bleaching is shown on Fig. 19. According to this data, band **I** is formed within the excitation pulse, approximately 1.5-2 ps. At the same time one would expect to observe the formation of bleaching of the CT band, but it actually appears with 3 ps delay after the excitation. This can be explained by the fact that there is another absorption band **III**, which overlaps with the CT band and is also formed within the excitation pulse. Thus bleaching of the CT band and the absorption of band **III** compensate each other resulting in zero absorbance difference. Subsequently, absorption band **III** decays and we start to observe bleaching of the CT band. This hypothesis is also supported by the kinetics of molecule **5**. The tails of the wide CT band of this molecule could be seen right after excitation. After a fast rise, transient absorption band **I** decays
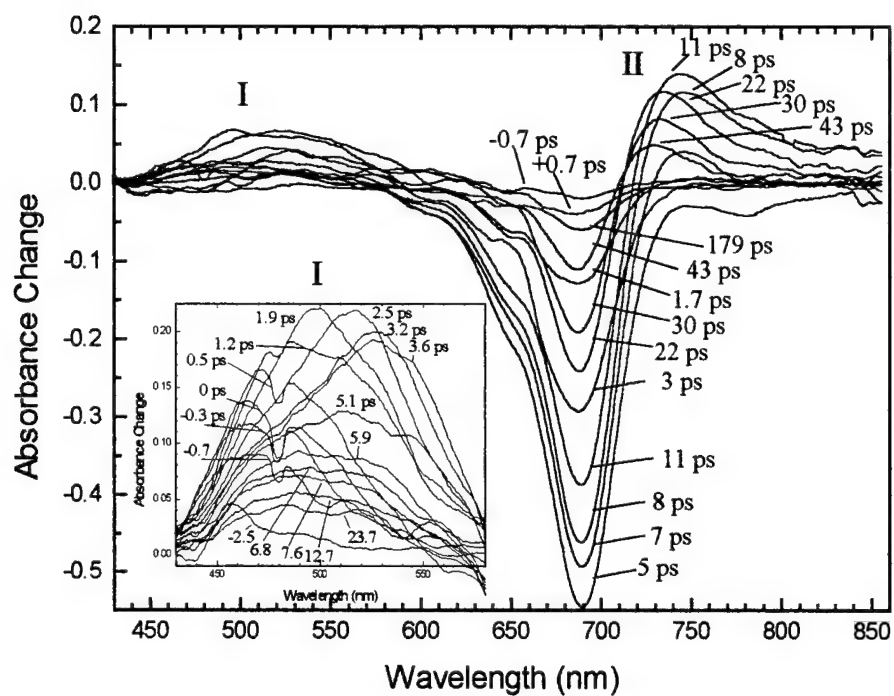
Fig.18: Absorbance change vs. wavelength at various times before and after excitation for molecule **6**
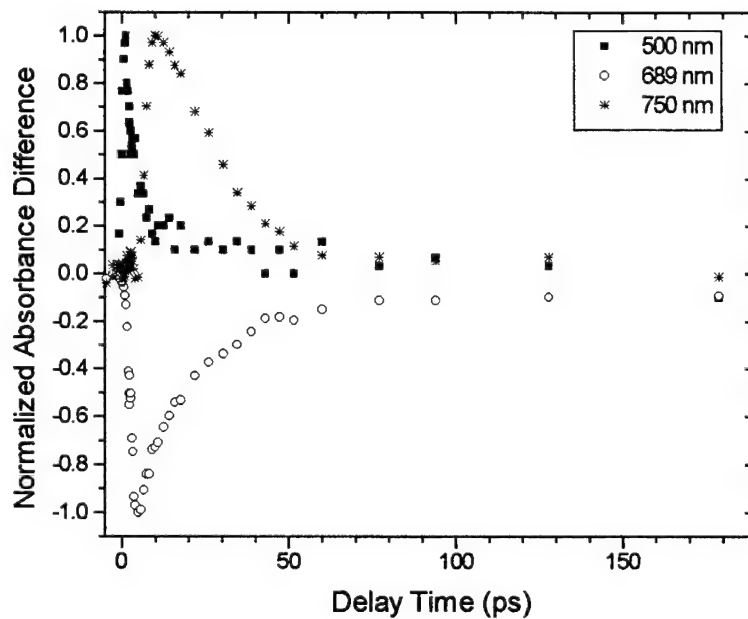

Fig.19: Kinetics of molecule **6** measured at three different wavelengths: 500 nm, 690 nm, and 750 nm

with 5 ps lifetime. At this time we also observe the development of band **II**, which is formed approximately with the same rate as the decay of band **I**. Band **II** decays with a lifetime constant of 19 ps, which coincides with the decay time constant of bleaching. Bleaching, however, does not vanish completely. This suggests to us that there are some parallel irreversible decay processes, which makes up 10% of initially excited molecules. From the above kinetic data we can deduce the following mechanism of light absorption:

$$A \underset{}{\overset{h\nu}{\rightleftharpoons}} A^* \xrightarrow{5\,ps} X \xrightarrow{19\,ps} A$$
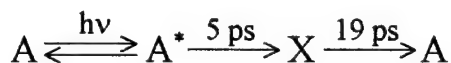
Where A is a ground state of the molecule; A^* is the excited state, which is represented by band **I** and **III**; X is a transient energy state. The decay time of band **I**, which corresponds to the lifetime of level A^*, was found to be sensitive to the polarity of the solvent. In more polar solvents this decay time tends to be shorter. However, the kinetic characteristics of bleaching and band **II** do not depend on the solvent polarity. From this effect we can draw the conclusion that A^* state is a charge transfer state, while state X is not a polar intermedium. In order to understand the nature of state X some additional experiments and calculations are required.

The other azulenic molecules studied showed the same behavior as molecule 6, which we have just discussed, except that band **II** in molecules **7-10** is shifted to near infrared, where the sensitivity of our detecting system is low. Therefore we were not able to observe this band in molecules **7-10**.
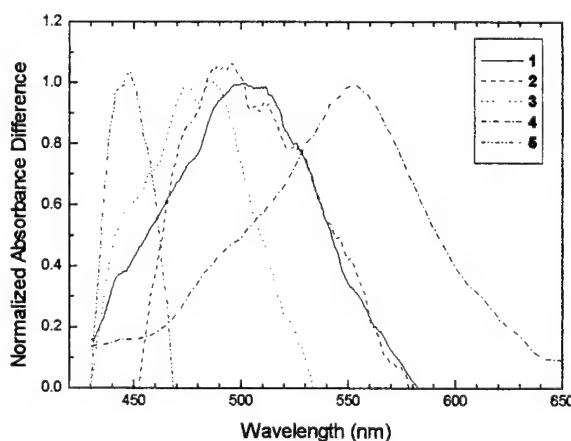

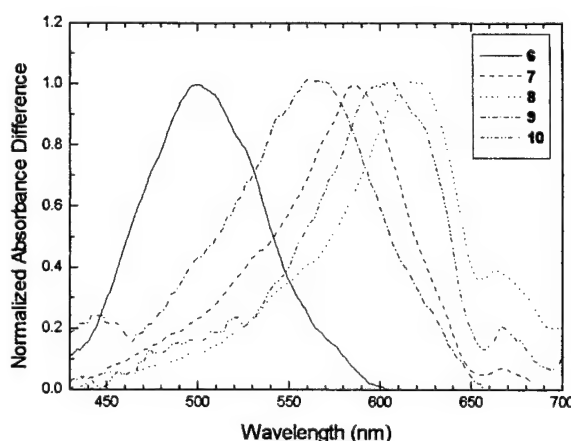Fig.20. Normalized spectra of band I for molecules **1-5**

Fig.21. Normalized spectra of band I for molecules **6-10**

Because of its spectral properties, namely, large cross section and fast kinetics band **I** can be utilized for power limiting applications. Figs. 20 and 21 show normalized spectra of band **I** for ten azulenes studied. The width of the band is between 40–100 nm and the absorption maximum wavelength varies from 450 to 620 nm. As it seen from Fig. 20 and

27

21, the RSA in these azulenes can cover a very wide segment of the visible spectrum especially when a mixture of several of these molecules is used. In Table 2, we have listed the spectral and kinetic characteristics of band **I** for all molecules studied. Using the cloranil data for calibration we measured the transient spectra and then calculated the transient absorption cross sections for the azulenes. The excited state cross sections at the maximum absorbance difference for azulenic molecules varies form 2.85×10^{-17} cm^2 for molecule **5**, to 13.3×10^{-17} cm^2 for molecule **7**. Molecule **7**, also has the highest cross section ratio σ_{ex}/σ_{gr}, equal to 10.8 at this wavelength. Band **I** rises with the rate of the excitation pulse in all of the azulenes. However, the decay time of this band depends on the molecule. It varies from 3 ps for molecule **1**, to 59 ps for molecule **2**. Therefore from the optical device point of view the onset of the "light limiting" is in the subpicosecond range and the return to clear vision in the tens of ps range. These basic data suggests that these types of molecules have indeed potential for use as optical limiting media.

Table 5: Characteristics of transient band **I** for azulenic molecules in dichloromethane

Molecule	λ_{max} , nm	Decay time, ps	$\sigma_{ex}(\lambda_{max})$, $10^{-17} \cdot$cm^2	$\sigma_{gr}(\lambda_{max})$, $10^{-17} \cdot$cm^2	σ_{ex}/σ_{gr}
1	500	3	4.49	1.73	2.6
2	500	59	3.53	2.87	1.2
3	480	34	3.07	1.31	2.4
4	555	11	8.69	1.43	6.1
5	450	27	2.85	1.35	2.1
6	500	5	3.44	1.00	3.4
7	588	31	13.3	1.24	10.8
8	620	48	11.4	1.96	5.8
9	560	8	3.75	1.50	2.5
10	605	25	6.49	1.70	3.8

VII. Conclusion

We have developed a new two-dimensional Z-scan technique, which uses a two-dimensional CCD detector to measure accurately and easier the nonlinear optical properties of materials using any arbitrary incident beam shape and sample thickness. With the aid of the split step beam propagation method, the beam distribution within the nonlinear media can be calculated with good accuracy anywhere inside the sample. This method also offers simple means for optimizing the figure of merit of optical limiters.

We have studied the nonlinear optical properties, picosecond photochemistry and transient species states and spectra of several NLO molecules, which include six metallobenzoporphyrins and ten donor-acceptor azulenic molecules using our two-dimensional Z-scan technique and picosecond transient spectroscopy. The data indicate that many of these molecules have strong nonlinear absorption in the broad region of the visible spectrum, and fast response time, which makes them suitable for power limiting applications.

VIII. Acknowledgment

IX. References

1. D.J. Hagan, T. Xia, A.A. Said, T.H. Wei, and E.W. Van Stryland, "High dynamic range optical limiters," Int. J. Nonlinear Opt. Phys. **2**, 483 (1993).
2. J.W. Perry, K. Mansour, I.-Y S. Lee, X.-L. Wu, P.V. Bedworth, C.-T. Chen, D.Ng, S.R. Marder, P. Miles, T. Wada, M. Tian, and H. Sasabe, "Organic optical limiter with a strong nonlinear absorptive response," Science, **273**, 1533 (1996).
3. W. Blau, H. Byrne, W.M. Dennis, J.M. Kelly, "Reverse saturable absorption in tetraphenylporphyrins," Opt. Commun. **56**, 25 (1985)
4. S. Guha, K. Kang, P. Porter, J.E. Roach, D.E. Remy, F.J. Aranda, D.V.G.L.N. Rao, "Third-order optical nonlinearities of metallotetrabenzoporphyrins and a platinum poly-yne," Opt. Lett. **17**, 264 (1992).
5. G.S. He, J.D. Bhawalkar, C.F. Zhao, and P.N. Prasad, "Optical limiting effect in a two-photon absorption dye doped solid matrix," Appl. Phys. Lett. **67**, 2433 (1995).
6. J.S. Shirk, R.G.S Pong, F.J. Bartoli, A.W. Snow, "Optical limiter using a lead phthslocyanine," Appl. Phy. Lett. **63**, 1880 (1993).
7. P. Chen, I.V. Tomov, M. Nakashima, J.F. Roach, and P.M. Rentzepis, "A two dimensional Z-scan method for the measurements of optical nonlinear effects", in Nonlinear Optical Liquids and Power Limiters, C. M. Lawson ed., Proc. SPIE **3146**, (1997)
8. B.L. Justus, A.L. Huston, A.J. Campillo, "Broadband thermal optical limiter", *Appl. Phys. Lett.* **63**, pp. 1483-1485, 1993
9. M. Sheik-Bahae, A.A. Said, T.H. Wei, D.J. Hagan, and E.W. Van Stryland, "Sensitive measurement of optical nonlinearities using a single beam," IEEE J. Quantum Electron. **26**, 760 (1990).
10. A.A. Said, M. Sheik-Bahae, D.J. Hagan, T.H. Wei, J. Wong, J. Young and E.W. Van Stryland. "Determination of bound-electronic and free-carrier nonlinearities in ZnSe, GaAs, CdTe and ZnTe," J. Opt. Soc. Am. **B9**, 405 (1992).
11. W. Zhao, and P. Palffy-Muhoray, "Z-scan measurement of $\chi^{(3)}$ using top-hat beams," Appl. Phys. Lett. **63**, 1613 (1993).
12. W. Zhao, and P. Palffy-Muhoray, "Z-scan technique using top-hat beams," Appl. Phys. Lett. **65**, 673 (1994).
13. T. Xia, D. J. Hagan, M. Sheik-Bahae, and E. W. Van Stryland, "Eclipsing Z-scan measurement of $\lambda/10^4$ wave-front distortion," Opt. Lett. **19**, 317 (1994).
14. M. Sheik-Bahae, A.A. Said, D.J. Hagan, M.J. Soileau, and E.W. Van Stryland, "Nonlinear refraction and optical limiting in thick media," Opt. Eng. **30**, 1228 (1991).
15. J.A. Hermann and R.G. McDuff, "Analysis of spatial scanning with thick optically nonlinear media," J. Opt. Soc. Am. **B10**, 2056 (1993).

16. P.B. Chapple, J. Staromlynska, and R.G. McDuff, "Z-scan studies in the thin- and the thick-sample limits," J. Opt. Soc. Am. **B11**, 975 (1994)

17. S. Hughes, and J.M. Burzler, "Theory of Z-scan measurements using Gaussian-Bessel beams," Phys. Rev. **A56**, R1103 (1997).

18. A. Marcano O., H. Maillotte, D. Gindre, and D. Metin, "Picosecond nonlinear refraction measurement in single-beam open Z-scan by charge-coupled device image processing," Opt. Lett. **21**, 101 (1996).

19. F. E. Hernandez, A. Marcano O., and H. Maillotte, "Sensitivity of the total beam profile distortion Z-scan for the measurement of nonlinear refraction," Opt. Comm. **134**, 529 (1997).

20. S. Hughes, J.M. Burzler, G. Spruce, and B.S. Wherrett, "Fast Fourier transform techniques for efficient simulation of Z-scan measurements," J. Opt. Soc. Am. **B12**, 1888 (1995).

21. J.M. Burzler, S. Hughes, and B.S. Wherrett, "Split-step Fourier methods applied to model nonlinear refractive effect in optically thick media," Appl. Phys. **62**, 389 (1996).

22. T. Okoshi, and S. Kitazawa. Analysis Methods for Electromagnetic Wave Problems, Edit. E. Yamashita. 341, Artech House, Boston (1990).

23. P. Chen, D.A. Oulianov, I.V. Tomov, and P.M. Rentzepis, "Two-dimensional Z scan for arbitrary beam shape and sample thickness", J. Appl. Phys. **85**, 7043-7050 (1999)

24. P. Chen, I.V. Tomov, M. Nakashima, J.F. Roach, and P.M. Rentzepis, "A two dimensional Z-scan method for the measurements of optical nonlinear effects", in Nonlinear Optical Liquids and Power Limiters, C. M. Lawson ed., Proc. SPIE **3146**, (1997)

25. D.J. Hagan, T.Xia, A.A. Said, A. Dogarius, and E.W. Van Stryland, "Optimization of reverse saturable absorber limiters: materials requirements and design consideration," in materials for optical limiting, R. Crane, K. Lewis, E. Van Stryland, and M. Khoshnevisan, eds., MRS symp. Proc. **374**, 161 (Materials Research Society, Boston, 1995).

26. P.A. Miles, "Bottleneck optical limiters: the optimal use of excited state absorbers," Appl. Opt. **33**, 6959 (1994).

27. Kaufmann, K.J.; Rentzepis, P. M. Acc. Chem. Res 1975, 8, 407.

28. Perry, J.W.; Mamsour, K.; Marder, S.R.; Perry, K.J.; Alvarez, D.; Choong, I. Opt. Lett. 1994, 19, 625.

29. Gouterman, M. J. Chem. Phys. 1959, 30, 1139.

30. Kobayashi, T.; Straub, K. D.; Rentzepis, P. M. Photochem. Photobiol. 1979, 29, 925.

31. Rodriguez, J.; Kirmaier, C.; Holten, D. J. Am. Chem. Soc. 1989, 111, 6500.

32. Ake, R. T.; Gouterman, M. Theoret. Chim. Acta. 1969, 15, 20.

33. Kobayashi, T.; Huppert, D.; Straub, K. D.; Rentzepis, P. M. J. Chem. Phys. 1979, 70, 1720.

34. Asano, M.; Kaizu, Y; Kobayshi, H. J. Chem Phys. 1988, 89, 6567.

35. Kim, D.; Holten, D.; Gouterman, M. J. Am. Chem. Soc, 1984, 106, 2793.

36. Hilinski, E.F.; Straub, K.D.; Rentzepis, P.M. Chem. Phys. Lett. 1984, 111, 333.

37. Ballard, S.G. Chem. Phys. Lett. 1983, 101, 177.

38. Ake, R.T.; Gouterman, M. Theoret. Chim. Acta. 1970, 17, 408 .

39. Chirvonyi, V. S.; Dzhagarov, B. M.; Timinskii, Y. V.; Gurinovich, G. P. Chem. Phys. Lett. 1980, 70, 79.
40. Kim, D.; Kirmaier, C.; Holten, D. Chem. Phys. 1983, 75, 305.
41. Kim, D.; Holten, D.; Gouterman, M.; Buchler, J.W.J. Am. Chem. Soc. 1984, 106, 4015.
42. Rodriguez, J. ; Holten, D. J. Chem. Phys. 1989, 91, 3525.
43. Ponterini, G.; Serpone, N.; Bergkamp, M.A.; Netzel, T.L. J. Am. Chem. Soc. 1983,105, 4639.
44. Kim, D.; Holten, D.; Gouterman, M.; Buchler, J.W.J. Am. Chem. Soc. 1984, 106, 4015.
45. H. Kobashi, T. Nagumo and T. Morita, "Hydrogen atom abstraction by *p*-chloranil triplet from tetrachlorohydroquinone and the presence of a competitive deactivation process," *Chem. Phys. Lett.* **57**, pp. 369-372, 1978
46. E.F. Hilinski, S.V. Milton, and P.M. Rentzepis, "Transient species in electron transfer: reaction of chloranil with donor aromatic compounds," *J. Am. Chem. Soc.* **105**, pp. 5193-5196, 1983
47. D.A. Oulianov, P. Chen, I.V. Tomov, P.M. Rentzepis, "Investigation of benzoporphyrin and azulenic compounds by two-dimensional z-scan technique", SPIE 3472, pp. 98-105, 1998
48. D.A. Oulianov , I.V. Tomov, A.S. Dvornikov, and P.M. Rentzepis, "Nonlinear properties and kinetics of some donor-acceptor optical limiting molecules, SPIE 3798, 1999
49. A.E. Asato, R.S.H. Liu, V.P. Rao, Y.M. Cai, "Azulene-containing donor-acceptor compounds as second-order nonlinear compounds," *Tetrahedron Letters* **37**, pp. 419-422, 1996
50. B.R. Kimball, M. Nakashima, B.S. DeCristofano, F.J Aranda, D.V.G.L.N Rao, "Third order nonlinear optics of some azulenic donor acceptor compounds", SPIE 3473, pp. 101-111, 1998
51. B.R. Kimball, M. Nakashima, B.S. DeCristofano, F.J Aranda, A.E. Asato, R.S.H. Liu, "Optical power limiting in some azulenic compounds", SPIE 3798, 1999.